Optoelectrical modeling of solar cells based on c-Si/a-Si:H nanowire arrays: focus on the electrical transport in between the nanowires

Alexandra Levtchenko, Sylvain Le Gall, Raphaël Lachaume, Jérôme Michallon, Stéphane Collin, José Alvarez, Zakaria Djebbour, Jean-Paul Kleider

Optoelectrical modeling of solar cells based on c-Si/a-Si:H nanowire arrays: focus on the electrical transport in between the nanowires

Optoelectrical modeling of solar cells based on c-Si/a-Si:H nanowire arrays: focus on the electrical transport in between the nanowires

Alexandra Levtchenko[1], Sylvain Le Gall[1]*, Raphaël Lachaume[1,2], Jérôme Michallon[1,2,3], Stéphane Collin[3], José Alvarez[1], Zakaria Djebbour[1†], and Jean-Paul Kleider[1]

[1] Génie électrique et électronique de Paris, UMR CNRS 8507, CentraleSupélec, Univ. Paris-Sud, UPMC, 11 rue Joliot-Curie, Plateau de Moulon 91192 Gif-sur-Yvette, France
[2] Institut Photovoltaïque d'Ile-de-France, 8 rue de la Renaissance, 92160 Antony, France
[3] Centre de Nanosciences et de Nanotechnologies, CNRS, Univ. Paris-Sud, C2N – Marcoussis, 91460 Marcoussis, France
[†]Département des Sciences Physiques, UVSQ, 45 av des Etats-Unis, 78035 Versailles, France

By coupling optical and electrical modeling, we have investigated the photovoltaic performances of p-i-n radial nanowires array based on crystalline p-type silicon (c-Si) core/hydrogenated amorphous silicon (a-Si:H) shell. By varying either the doping concentration of the c-Si core, or back contact work function we can separate and highlight the contribution to the cell's performance of the nanowires themselves (the radial cell) from the interspace between the nanowires (the planar cell). We show that the build-in potential (V_{bi}) in the radial and planar cells strongly depends on the doping of c-Si core and the work function of the back contact respectively. Consequently, the solar cell's performance is degraded if either the doping concentration of the c-Si core, or/and the work function of the back contact is too low. By inserting a thin (p) a-Si:H layer between both core/absorber and back contact/absorber, the performance of the solar cell can be improved by partly fixing the V_{bi} at both interfaces due to strong electrostatic screening effect. Depositing such a buffer layer playing the role of an electrostatic screen for charge carriers is a suggested way of enhancing the performance of solar cells based on radial p-i-n or n-i-p nanowire array.

* Corresponding author: sylvain.legall@geeps.centralesupelec.fr

1. Introduction

Semiconductor nanowires have attracted much attention in the last decade for their unique electronic properties and potential applications in several emerging areas such as electronic sensor, photovoltaic, thermoelectric, battery and biological applications [1]. Especially, silicon nanowires are under active investigation for photovoltaic applications because they offer novel approaches for solar to electric energy conversion leading to high-efficiency devices by simple manufacturing [2-4]. Due to their geometry, silicon nanowires provide excellent anti-reflection and light trapping effects [5, 6], which make this array of nanowires a promising candidate to lower both the required quality and quantity of silicon material. Moreover, radial p-n junctions obtained with the cylindrical structure allow to decouple light absorption along the wire axis and the carrier collection along the radial direction. Among other nanowire technologies, crystalline silicon (c-Si) nanowire based solar cells have been emerging [7] with high power conversion efficiency [8-10]. However, the technology based on crystalline silicon is an expensive mainly due to the manufacturing costs of processing, crystallization, purification *etc*. A good alternative for low cost solar cells is to use of the thin film technologies such as hydrogenated amorphous silicon (a-Si:H). In this regard, significant improvements in nanowire growth and material properties can be obtained by considering a c-Si core nanowires surrounded by an a-Si:H absorber shell forming a radial p-i-n heterojunctions [11-13].

Numerical simulations have revealed to be powerful tools to guide the ideal design of radial heterojunctions considered in nanowire based solar cells. For instance, optical modeling has been used to investigate the optical light harvesting properties [11, 14-16], while electrical modeling has been used to determine their electrical performance, but without taking into account the light enhancement effects due to nanostructuration [17, 18]. Very few articles rigorously take into account both the optical and electrical aspects [19]. Recently, we have developed a tool to couple electrical and optical simulators and we applied it on p-i-n radial nanowires based on c-Si core/a-Si:H shell heterojunction in order to simulate the electrical performance of solar cells when the light harvesting effect is taken into account in the photogeneration rate distribution of vertical nanowire arrays [20]. It was emphasized that the planar region between the nanowires has to be taken into account because it strongly influences the performance of the entire solar cell. In this study, we perform coupled optical/electrical modeling on the same structure, and show that the performance of the solar cell can be increased by inserting a thin (p) a-Si:H buffer layer in the stack.

2. Structure and modeling

The structure of interest is depicted in figures 1(a) and 1(b), and is similar to the one studied in our previous work [20]. The array of nanowires has been designed from experimental achievements [11-13]. For the modeling, a periodic square mesh arrangement was considered with a nanowire density of 2.6×10^8 cm^{-2} roughly equivalent to a period of 620 nm [12, 20]. Each nanowire, described in figure 1(b), consists in a radial p-i-n junction with 20 nm p-type crystalline silicon core, (p)c-Si, covered by 100 nm of intrinsic hydrogenated amorphous silicon absorber, (i)a-Si:H, surrounded by 10 nm of n-type hydrogenated amorphous silicon shell, (n)a-Si:H. The 1 µm long c-Si core allows the radial collection of holes which then flow to the back contact made of aluminium-doped zinc oxide (AZO). Radial collection of electrons is ensured by indium tin oxide (ITO). In addition to the radial junction for nanowires, the solar cell also integrates the planar junction in between the nanowires.

The electrical modeling was performed using TCAD software (ATLAS from Silvaco [21]) based on the finite volume method, which solves the physical equations self-consistently: Poisson and carrier continuity equations with the drift-diffusion transport. The mesh was reduced and refined close to the interfaces until a stable solution was obtained. Electrical parameters of the different semiconductor materials are gathered in Table 1. Amorphous silicon was modeled with a density of states (DOS) in the bandgap, consisting of two exponential tail state distributions (acceptor-like for the conduction band tail and donor-like for the valence band tail) and two Gaussian deep defect distributions representative of dangling bonds (one donor-type and the other acceptor-type). According to the

defect-pool model, the equilibrium DOS in a-Si:H depends on the position of the Fermi level [22], meaning that it should be non-homogeneous especially close to the core and the outer shell interfaces. However we checked that the changes in the DOS close to the interfaces did not have strong impact on the presented results and on the trends observed when varying the doping density in the c-Si core or the AZO work function. The input parameters for the DOS of the a-Si:H layers are reported in Table 2. More details about the electrical parameters of a-Si:H layers can be found elsewhere [20]. In the (p)c-Si core, recombination using both standard Shockley–Read–Hall and Auger models were taken into account and the electron and hole mobilities were also considered as doping dependent using a standard model [23, 24]. The work function of ITO was chosen to meet flat band conditions at the ITO/(n) a-Si:H interface in order to study only the influence of the AZO contact. The work function values of transparent conductive oxides (TCO) such as AZO depend on the measurement technique as well as on the material synthesis conditions [25, 26], therefore in this study it was varied by ±0.5 eV around 5 eV. Interfaces between the different layers were considered as ideal (no interface defects). The surface recombination velocities at the contacts were taken infinite for both types of carriers (no selective contacts for collection) [27].

Optical modeling was performed using a three-dimensional Rigorous Coupled Wave Analysis (RCWA) method in order to calculate the carrier photogeneration in the nanowire array. The optical indices of materials were directly extracted from ellipsometry measurements. In contrast with the electrical simulation where ITO and AZO are replaced by electric contact modelled by specific boundary conditions (work function and surface recombination velocities values), the optical simulation considers the bulk of both ITO and AZO materials (with optical indices). Photogeneration profile of a single nanowire extracted from optical simulation is then flattened to a 2D plane to be input in the electrical simulations [19, 20, 28, 29]. The photogeneration profile is shown in figure 1(c). As expected, this profile is different from the exponentially decreasing profile from the illuminated surface, as would be obtained from the simple Beer-Lambert absorption law**.** To realize the optical/electrical coupling, this photogeneration profile is then implemented into the TCAD simulator that exploits the radial symmetry of the nanowires. More details about the electrical and optical modeling and coupling can be found in our previous paper [20].

As shown in figures 1(a), 1(b) and 1(c), the studied structure is composed of two parts: a radial p-i-n cell in the nanowire and a planar p-i-n cell related to the interspacing in between the nanowires. The impact of each part on the performance of the entire solar cell is investigated by varying the doping of the p-type c-Si core and the back contact work function of AZO (W_{AZO}) as they determine the band-bending in the (i) a-Si:H absorber in the radial and planar part, respectively.

3. Results and discussion

The one-dimensional energy band diagrams at equilibrium computed along the cutline as defined in figure 2(a) for the radial and planar junctions are shown in figure 2 (b) and 2(c), respectively. For the radial junction, the band-bending is strongly impacted by the acceptor concentration (N_a) of the c-Si core. Indeed, the built-in potential (V_{bi}) increases, for instance, from 0.28 eV for $N_a=1\times10^{18}$ cm^{-3} to 1.05 eV for $N_a=8\times10^{18}$ cm^{-3} (figure 2(b)). The strong decrease of V_{bi} is not only related to the decrease of the doping core N_a but is also impacted by the thickness of the c-Si core because it limits the width of the space charge region (the number of acceptor charges is too low in the c-Si core with a radius of 20 nm). However, by increasing the c-Si core radius above ~100 nm, additional simulations (not shown) indicated that the V_{bi} follows the variation of the c-Si work function according to the doping concentration.

For the planar junction, V_{bi} in the absorber increases with increasing the AZO work function (W_{AZO}), as reported in figure 2(c). The change of the band-bending according to either N_a or W_{AZO}, and the competition between them, impact directly the photovoltaic performance of the entire solar cell. The evolution of the short-circuit current density (J_{sc}), open-circuit voltage (V_{oc}) and efficiency, for varying the doping of c-Si and W_{AZO}, are shown in figure 2 (d), 2(e) and 2(f) respectively. The

strong dependence of J_{sc} with the doping concentration of the c-Si core is due to the increase of V_{bi} in the absorber in the radial part, which increases the electric field and improves the charge carrier separation. An increase of V_{bi} also takes place in the absorber in the planar part by increasing the W_{AZO}. However, as the photogeneration rate is lower in the planar part in between the nanowire than in the nanowire, the carrier collection enhancement by the electric field has a weaker effect here, which explains the low W_{AZO} dependence of J_{sc} in the entire cell. So, this explains why J_{sc} is mainly influenced by the radial cell.

In figure 2(e), two behaviours can be distinguished for the evolution of V_{oc}. For W_{AZO}<5.0 eV, the V_{oc} increases linearly with W_{AZO}, independently of N_a values. The strong impact of W_{AZO} on V_{oc} is due to the increase of V_{bi} in the absorber in the planar region, meaning that V_{oc} is mainly influenced by the planar cell. On the contrary, for W_{AZO} > 5.0 eV, V_{bi} of the absorber is lower in the radial junction as compared to the planar one, leading to N_a dependence of V_{oc}. Indeed, the increase of W_{AZO} leads to a decrease of the dark current density mainly driven by the planar region [20], which explains the drop in V_{oc}. Thus, for low W_{AZO} values, V_{oc} of the entire cell is degraded due to the planar region.

The efficiency values in figure 2(f) are driven by the evolution of V_{oc}. So it appears that the planar junction can drastically affect the performance of the solar cell, mainly for lowly doped c-Si core and AZO back contact having a low work function value.

In order to remove the dependence of the core doping and back contact work function on the solar cell efficiency, a thin buffer layer of p-type a-Si:H at the AZO/absorber interface (and also at the core/absorber interface) as depicted in figure 3(a), is now investigated. This buffer layer is modeled by a 10 nm thick (p) a-Si:H with input electrical parameters reported in Table 1 and the DOS from Table 2. To keep the same thickness of 100 nm for the absorber layer as for the reference structure, the thickness of the (i) a-Si:H layer is thus reduced to 90 nm.

The one-dimensional energy band diagrams at equilibrium for the radial and planar junctions for the new structure are shown in figure 3 (b) and 3(c) respectively at the exact same position as compared to the reference structure (figures 2(b) and 2(c)). For the radial junction, we notice that the band-bending is not influenced by N_a values. Contrary to the reference structure without (p) a-Si:H layer, V_{bi} is fixed by the pinning of the Fermi level in the (p) a-Si:H layer *i.e* V_{bi} is fixed due to the electrostatic screening effect provided by the numerous charged defects of the inserted highly doped (p) a-Si:H layer [27]. Indeed, we can estimate the Debye screening length $L_D=(\varepsilon/q^2N(E_F))^{1/2}$ around 4.5 nm in this (p) a-Si/H buffer layer (here $N(E_F)\sim3\times10^{19}$ cm^{-3} is the DOS at Fermi level) which is good agreement as in reference [30]. In other words, as long as this supplementary layer thickness is several times L_D, V_{bi} is rather not influenced by the c-Si contact work function, and nearly all the voltage drop induced by a change of c-Si doping is taken in the (p) a-Si:H layer [26]. Similarly to the band diagram for the planar junction of figure 3(c), the position of conduction (E_c) and valence (E_v) bands at the border of AZO (depth of 110 nm) is fixed by the W_{AZO} values. The inserted buffer layer increases E_c and E_v values near the AZO metal for the lower W_{AZO}. Consequently, a curvature in the band-bending can appears close to the interface, as seen for instance for W_{AZO}=4.8 eV. The maximum value of V_{bi} in the absorber is thus higher in the planar junction with the additional p-type a-Si:H layer even by electrostatic screening effect. For W_{AZO} > 5.2 eV, this buffer layer has no impact on the band diagram (linear bands in the absorber as in the case of the reference layer studied in figure 2(c)).

The variation of J_{sc} for the new structure with (p) a-Si:H buffer layer is shown in figure 3(d). We notice that J_{sc} remains constant because the maximum V_{bi} in the absorber (so the electric field) is independent of the doping of the c-Si core, as reveal in figure 3(b). The electric field in the absorber is now fixed by the work function of the additional (p) a-Si:H layer. Consequently, J_{sc} is not anymore

affected by the radial contact contrary to the structure without buffer layer. The J_{sc} values lie between 12.9 and 13.1 mA/cm² for W_{AZO} in the range of 4.8-5.5 eV. These values are slightly higher than the values (11.2-12.9 mA/cm²) of the reference structure observed previously in figure 2(d). On the other hand, the increase of V_{oc} as a function of W_{AZO} is smaller than for the reference structure and reaches a saturated value around 0.85 V, as shown in figure 3(e). The structure with the buffer layer thus becomes less sensitive to the planar contact due to the screening effect of the (p) a-Si:H layer. This buffer layer thus helps to increase the V_{oc} as long as its effective work function remains higher than W_{AZO}. Finally, evolutions of the efficiencies are plotted in figure 3(f) for the reference (line) and the new structure with the additional buffer layer (symbol). The efficiency is improved with the buffer layer at low W_{AZO} due to V_{oc} higher. However, if W_{AZO} is high enough to allow the major part of the dark current to flow through the radial junction, the buffer layer will limit the solar cell performance (if the c-Si core doping is too high).

The inserted buffer layer, due to screening effect, has a strong impact on the solar cell performance. In the following, we have investigated the strength of the screening effect by modifying the DOS of the (p) a-Si:H layer in the structure. In figures 4, we show the influence of the activation energy E_a (*i.e* the Fermi level position from E_V) of the (p) a-Si :H buffer layer on the equilibrium band-bending. In both the radial (figure 4(a)) and planar (figure 4(b)) junctions, the maximum V_{bi} in the absorber increases when E_a decreases. Basically, a lower value of E_a means a higher doped-layer (or more defective layer) which increases the V_{bi} (due to increase of work function difference between the back and front contact). In a more defective layer, L_D is reduced which enhances the screening effect. This effect is even stronger for the lowly doped core and lower $W_{AZO.}$ In contrast to a thin c-Si buffer layer, the a-Si:H material develops a strong charge due to the huge DOS at the Fermi Level, so a thin layer is enough for having a strong electrostatic screening effect.

Experimentally, S. Misra *et al.* (2013) [11] have deposited an additional 10 nm thick p-type a-Si:H layer at both c-Si core/(i) a-Si:H absorber and AZO/absorber interfaces for the same p-i-n nanowire stack. They claimed that this inserted layer allows to rise the V_{oc} of 0.05 V, for a maximal value of 0.85 V. They explained this raise of V_{oc} by the reduction of the recombination rate at p-i interface. In this study, we provide another explanation: the electrostatic screening effect of this (p) a-Si:H layer. Note that the maximum simulated J_{sc} (13.1 mA/cm²) and V_{oc} (0.85 V) values are very close to that obtained experimentally by S. Misra *et al.* (2013) [11].

4. Conclusion

In summary, we have investigated the performance of a radial c-Si core/a-Si:H absorber shell nanowire array by coupling optical and electrical modeling. We show that the built-in potential V_{bi} of the radial and planar junction strongly depends of the doping of c-Si core and the work function of the AZO back contact. Consequently, the solar cell's performance is degraded if the c-Si core is not doped enough and the work function of the AZO back contact too low. By inserting a thin (p) a-Si:H buffer layer in between both core/absorber and absorber/AZO interfaces, we show that V_{bi} in both radial and planar junctions is mainly fixed by this buffer layer due to the strong electrostatic screening effect. This screening effect is stronger if the thin buffer have a higher density of state in the bandgap (*i.e* if the (p) a-Si:H is more defective). Consequently, the performance of the solar cell is enhanced because: (i) the J_{sc} remains constant with a value higher than obtained in the structure without the buffer layer, independently of the core doping, and (ii) the V_{oc} increases as long as its work function remains higher than the AZO one. The deposition of a thin defective buffer layer playing the role of electrostatic

screening for charge carriers, if the required growth both c-Si core doping and back contact quality conditions are not fulfill, should be a cunning way to increase the solar performance of p-i-n or n-i-p radial a-Si:H-based nanowires solar cells.

Acknowledgements
The authors acknowledge the financial support from the French Research National Agency – project SOLARIUM (ANR-14-CE05-0025).

References

[1] N. P. Dasgupta, J. Sun, C. Liu, S. Brittman, S. C. Andrews, J. Lim, H. Gao, R. Yan, and P. Yang, *Adv. Mater.* **26**, 2137 (2014).

[2] R. Ghosh and P. K. Giri, *Nanotechnol.* **28**, 0120001 (2017).

[3] K.-Q. Peng and S.-T. Lee, *Adv. Mater.* **23**, 198 (2011).

[4] F. Priolo, T. Gregorkiewicz, M. Galli and T. F. Krauss, *Nat. Nanotechnology* **9**, 19 (2014).

[5] L. Hu and G. Chen, *Nano Lett.* **7,** 3249 (2007)

[6] E. Garnett and P. Yang, *Nano Lett.* **10,** 1082 (2010)

[7] T. Stelzner, M. Pietsch, G. Andra, F. Falk, E. Ose1 and S. Christiansen, *Nanotechnol.* **19**, 295203 (2008).

[8] X. X. Lin, X. Hua, Z. G. Huang and W. Z. Shen, *Nanotechnol.* **24**, 235402 (2013).

[9] M-D. Ko, T. Rim, K. Kim, M. Meyyappan and C-K. Baek, *Sci. Rep.* **5**, 11646 (2015).

[10] X. X. Lin, Y. Zeng, S. H. Zhong, Z. G. Huang, H. Q. Qian, J. Ling, J. B. Zhu and W. Z. Shen, *Nanotechnol.* **26**, 125401 (2015).

[11] S. Misra, L. Yu, M. Foldyna, and P. Roca i Cabarrocas, *IEEE Journal of Photovoltaics* **5**, 40 (2015).

[12] S. Misra, L. Yu, M. Foldyna, and P. Roca i Cabarrocas, *Sol. Energy Mater. Sol. Cells* **118**, 90 (2013).

[13] S. Misra, M. Foldyna, I. Florea, L. Yu, and P. Roca i Cabarrocas, *MRS Proceedings* 1770, 73 (2015).

[14] L. Yu, S. Misra, J. Wang, S. Qian, M. Foldyna, J. Xu, Y. Shi, E. Johnson, and P. Roca i Cabarrocas, *Sci. Rep.* **4**, 4357 (2014).

[15] S. Qian, S. Misra, J. Lu, Z. Yu, L. Yu, J. Xu, J. Wang, L. Xu, Y. Shi, K. Chen, and P. Roca i Cabarrocas, *Appl. Phys. Lett.* **107**, 043902 (2015).

[16] H. Ferhati, F. Djeffal, D. Arar, and Z. Dibi, *Phys. Status Solidi C* **2017**, 1700146 (2017).

[17] Z. Pei, S-T. Chang, C-W. Liu, and Y-C. Chen, *IEEE Electron. Device Lett.* **30**, 1305 (2009).

[18] D. Diouf, I. Ngo, J-P. Kleider, M. Gueunier-Farret, and J. Alvarez, *Phys. Status Solidi A* **209**, 1026 (2012).

[19] M. Zanuccoli, I. Semenihin, J. Michallon, E. Sangiorgi, C. Fiegna, *J. Comput. Electron* **12**, 572 (2013)

[20] A. Levtchenko, R. Lachaume, J. Michalon, S. Collin, J. Alvarez, S. Le Gall, Z. Djebbour, and J-P. Kleider, *Phys. Status Solidi C* **14**, 1700181 (2017)

[21] User's manual for ATLAS from Silvaco International.

[22] M. J. Powell and S. C. Deane, *Phys. Rev. B* **48**, 10815 (1993).

[23] J. Dziewior, W. Schimid, Appl. Phys. Lett. 31, 349 (1977).

[24] M. E. Law, E. Solley, M. Liang, D. E. Burk, *IEEE Electron. Device Lett.* **12**, 401 (1991).

[25] M. D. Kelzenberg, M. C. Putnam, D. B. Turner-Evans, N. S. Lewisand, H. A. Atwater, in: *Proceedings of the 34th IEEE Photovoltaic Specialists Conference (PVSC)*, Philadelphia, CA, USA, 2009, pp. 001948–001953.

[26] R. Lachaume, W. Favre, P. Scheiblin, X. Garros, N. Nguyen, J. Coignus, D. Munoz, G. Reimbold, *Energy Procedia* **38**, 770 (2013).

[27] R. Lachaume thesis "Contribution to the electrical characterization and to the numerical simulatio,n of the silicon heterojunction solar cells », PhD Thesis (French) 2014, Grenoble Univ., https://tel.archives-ouvertes.fr/tel-01186474.

[28] R. Jaramillo, and S. Ramanathan, *Sol. Energ.Mater. Sol. Cells* **95**, 602, 2011.

[29] J. Michallon, D. Bucci, A. Morand, M. Zanuccoli, V. Consonni, A. Kaminski-Cachopo, *Opt. Express* **22**, A1174 (2014)

[30] R. Varache, J-P. Kleider, W. Favre, L. Korte, *J. Appl. Phys.* **112**, 123717 (2012)

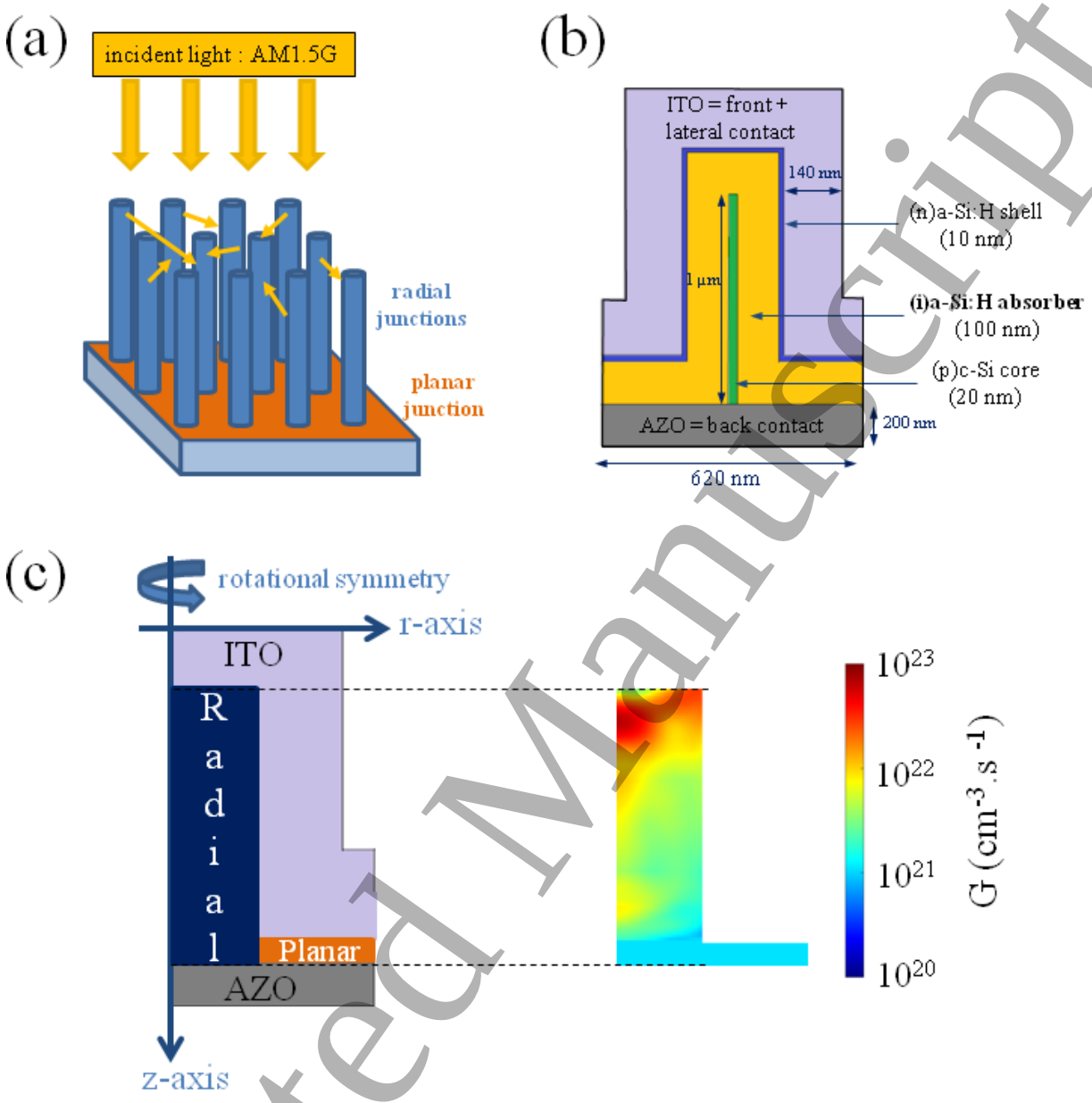

Figure 1: Sketches of (a) the simulated nanowire array highlighting the radial and planar junction,(b) detailed structures of a single nanowire that has been modelled and (c) the radial symmetry of nanowires with the corresponding photogeneration rate distribution G calculated by RCWA.

Table 1. Input electrical parameters of materials at 300K

	(p) c-Si	(i) a-Si:H	(n) a-Si:H	(p) a-Si:H
E_g (eV)	1.12	1.7	1.7	1.7
χ (eV)	4.05	3.8	3.8	3.8
ε_r	11.9	11.9	11.9	11.9
μ_n (cm²/(V.s))	675 – 99.5*	20	20	20
μ_p (cm²/(V.s))	331.5 – 66.5*	4	4	4
N_c (cm^{-3})	2.8×10^{19}	5×10^{20}	5×10^{20}	5×10^{20}
N_v (cm^{-3})	1.04×10^{19}	5×10^{20}	5×10^{20}	5×10^{20}

* For doping range 1×10^{17} - 8×10^{18} cm^{-3}

Table 2. Input electrical parameters of density of states in (n) ; (i) and (p) type a-Si :H. The parameters N_G , ω_G , and E_G correspond, respectively, to the trap density, characteristic energy width, and energy position referred to the valence band edge, of the Gaussian distribution. The parameters $\sigma_{G,e}$, $\sigma_{G,h}$ are, respectively, the capture cross-sections for electrons and holes, of the Gaussian distribution. Similarly, all the parameters with a T-index correspond to the same physical quantities but in the tail distributions.

		(n) a-Si:H		(i) a-Si:H		(p) a-Si:H	
		donor	accept	donor	accept	donor	accept
Tail distribution	N_T (cm^{-3}/eV)	2×10^{22}	2×10^{22}	10^{21}	10^{21}	2×10^{22}	2×10^{22}
	ω_T (meV)	60	23	43	26	60	34
	$\sigma_{T,e}$ (cm²)	10^{-15}	10^{-17}	10^{-16}	10^{-17}	10^{-16}	10^{-17}
	$\sigma_{T,h}$ (cm²)	10^{-17}	10^{-15}	10^{-17}	10^{-16}	10^{-17}	10^{-16}
Gaussian distribution	N_G (cm^{-3}/eV)	2.35×10^{19}	2.35×10^{19}	3×10^{15}	3×10^{15}	1.2×10^{20}	1.2×10^{20}
	ω_G (meV)	270	270	270	270	270	270
	E_G (meV)	650	850	600	800	1250	250
	$\sigma_{G,e}$ (cm²)	10^{-15}	10^{-17}	10^{-16}	10^{-17}	10^{-16}	10^{-17}
	$\sigma_{G,h}$ (cm²)	10^{-17}	10^{-15}	10^{-17}	10^{-16}	10^{-17}	10^{-16}
Doping	N_a , N_d (cm^{-3})	1.7×10^{19}	-	-	-	-	5.9×10^{19}
Fermi level position* from E_v	E_a (eV)	1.54		0.85		0.39	

* Also named activation energy

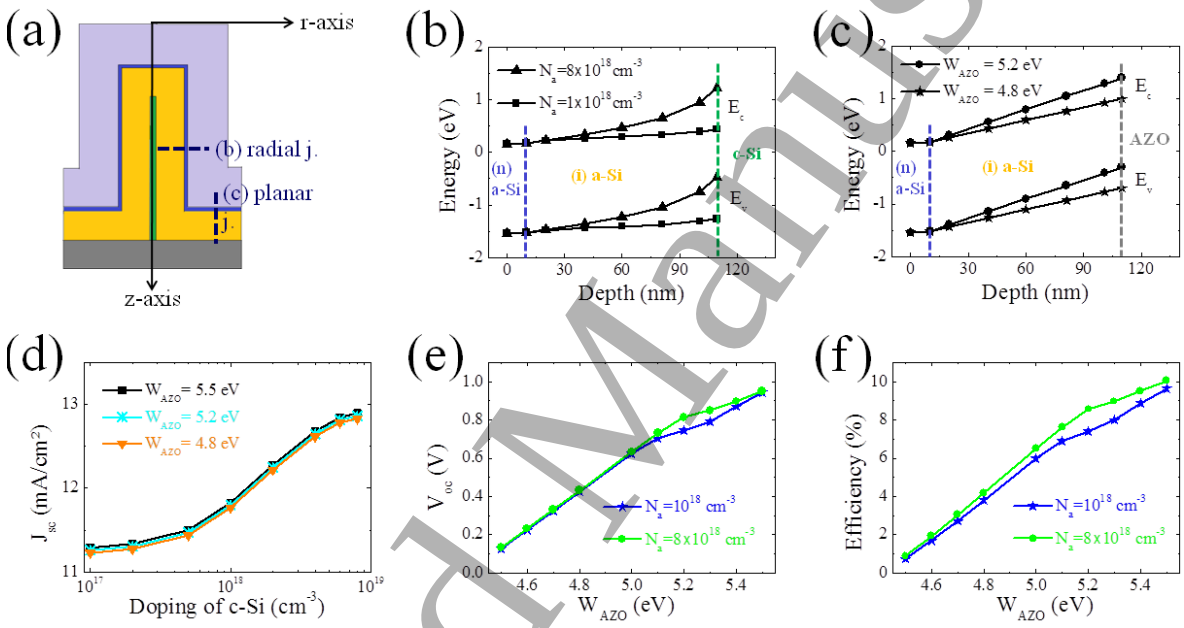

Figure 2: Photovoltaic parameters and band diagrams of the nanowire structure. (a) Sketch of simplified structure with the cutlines for extracting the one-dimensional band diagrams. (b) Energy band diagram at equilibrium across the (n) a-Si:H/(i) a-Si:H/c-Si radial junction for two c-Si doping concentrations (square : 1×10^{18} cm^{-3} and triangle: 8×10^{18} cm^{-3}). (c) Energy band diagram at equilibrium across the (n) a-Si:H/(i) a-Si:H/AZO planar junction for two AZO work functions (star : 4.8 eV and circle: 5.2 eV). (d) Variation of J_{sc} *versus* doping concentration of c-Si layer for three work function values (black square: 5.5eV ; cyan cross: 5.2 eV and orange triangle: 4.8 eV). (e) Variation of V_{oc} and (f) efficiency as the function of AZO work function with varying two doping concentration values (blue star : 1×10^{18} cm^{-3} and green circle : 8×10^{18} cm^{-3}).

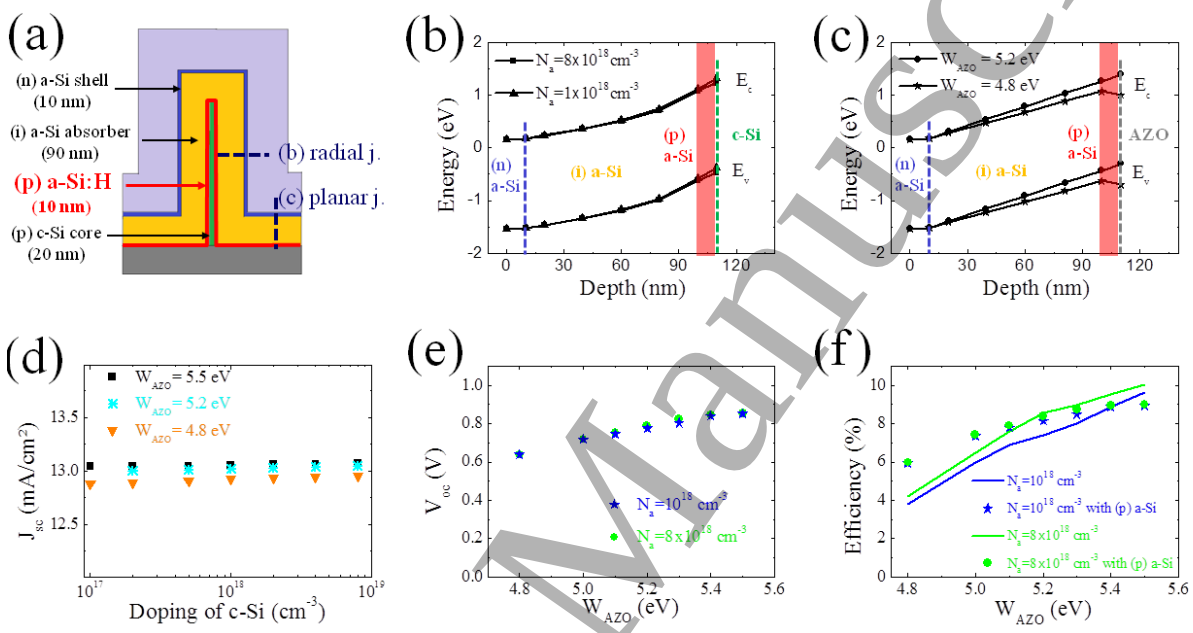

Figure 3: Photovoltaic parameters and energy band diagrams of the nanowire structure with an additional (p) a-Si:H buffer layer inserted. (a) Sketch of the modeled structure with the cutlines for extracting one dimensional band diagrams. (b) & (c) Energy band diagrams at equilibrium across (b) the (n) a-Si:H/(i) a-Si:H/(p) a-Si:H/c-Si radial junction for two c-Si doping concentrations (square : 1×10^{18} cm^{-3} and triangle : 8×10^{18} cm^{-3}) and (c) the (n) a-Si:H/(i) a-Si:H/(p) a-Si:H/AZO planar junction for two AZO work functions (star : 4.8 eV and circle : 5.2 eV). (d) Variation of J_{sc} against doping concentration of c-Si layer for three work function values (black square : 5.5 eV ; cyan cross : 5.2 eV and orange triangle : 4.8 eV) (e) Variation of V_{oc} and (f) efficiency as the function of AZO work function with varying two doping concentration values (blue star : 1×10^{18} cm^{-3} and green circle : 8×10^{18} cm^{-3}). The line curves represent the efficiencies of the nanowire structure without (p) a-Si:H buffer layer for the same doping concentration values (blue line: 1×10^{18} cm^{-3} and green line: 8×10^{18} cm^{-3}).

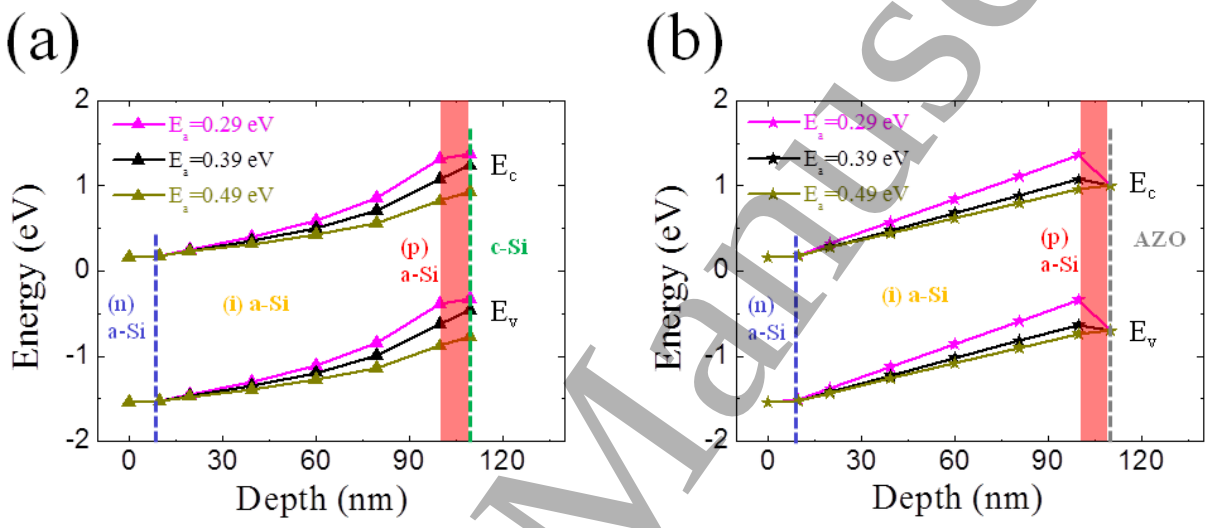

Figure 4: Influence of the activation energy E_a of the (p) a-Si:H buffer layer on the one-dimensional energy band diagrams at equilibrium for (a) radial junction with core doping concentration of $N_a=1\times10^{18}$ cm^{-3} and for (b) planar junction with AZO work function of $W_{AZO}=4.8$ eV.